Polymer Degradation and Stability 197 (2022) 109865

Contents lists available at ScienceDirect

Polymer Degradation and Stability

journal homepage: www.elsevier.com/locate/polymdegradstab

PLA/CaO nanocomposites with antimicrobial and photodegradation properties

Carlos Loyo[a], Viviana Moreno-Serna[a,*], Jairo Fuentes[a], Nicolás Amigo[a], Francesca Antonella Sepúlveda[a], J. Andrés Ortiz[a,b], Lina M. Rivas[c], María Teresa Ulloa[d], Rosario Benavente[e], Paula A. Zapata[a,*]

[a] Universidad de Santiago de Chile (USACH), Facultad de Química y Biología, Departamento de Ciencias del Ambiente, Grupo Polímeros, Santiago, Chile
[b] Departamento de Ingeniería Química, Biotecnología y Materiales, Facultad de Ciencias Físicas y Matemáticas, Universidad de Chile, Avenida Beaucheff 851, Santiago, Chile
[c] Genomics and Resistant Microbes (GeRM) Group, Clínica Alemana, Universidad del Desarrollo, Santiago, Chile
[d] Programa de Microbiologiá y Micologiá, ICBM-Facultad de Medicina Universidad de Chile, dirección, Avenida Independencia 1027, Comuna Independencia, Santiago, Chile
[e] Instituto de Ciencia y Tecnologiá de Polimeros, ICTP-CSIC, Juan de la Cierva, 3. 28006 Madrid, Spain

ARTICLE INFO

Article history:
Received 21 September 2021
Revised 30 December 2021
Accepted 6 February 2022
Available online 8 February 2022

Keywords:
Poly(lactic acid) (PLA)
CaO nanoparticles
Modified nanoparticles
Nanocomposites
Antimicrobial
Photodegradation

ABSTRACT

CaO nanoparticles sized ca. 26 nm were organically modified with oleic acid (Ol-CaO), and both were incorporated into PLA at concentrations of 5 and 8 wt.% by a melting process. Modification of nanoparticles improved the distribution into PLA, as seen by transmission electron microscopy (TEM). Thermal analysis revealed that the presence of Ol-CaO in the PLA matrix promoted a decrease ca. 13% in the glass transition temperature (T_g). The thermal stability of the PLA/Ol-CaO decreased ca. 23% compared to the neat PLA due to the catalytic activity from nanoparticles, while Vickers Microhardness (HV) for nanocomposites PLA/Ol-CaO increased ca. 9%, compared with the neat PLA, due to the good dispersion of modified-surface Ol-CaO nanoparticles in PLA. PLA/Ol-CaO nanocomposites reached 99.9% of antimicrobial effectiveness against *E. coli* for nanoparticles content above 8 wt.%. From photodegradation tests under irradiation during five days, it was verified that the presence of CaO nanoparticles accelerated the photodegradation of the polymer matrix nanoparticles into PLA promoted a decreasing ca. 13% of Tg and an increase in the degree of crystallinity (Xc) (ca. 7%), compared to PLA/CaO without irradiation. Besides, the viscosity molecular weight ($\bar{M}v$) of PLA/CaO showed a higher decrease than neat PLA after irradiation, and SEM analysis showed that the nanocomposites presented cavities around the nanoparticles after irradiation. Our results showed that incorporating CaO nanoparticles into the PLA polymer matrix allows future development of more sustainable materials as nanocomposites for food packaging or medical devices.

1. Introduction

Over the recent decades, the use of petroleum-based polymers has increased considerably due to versatility, low-cost production, and excellent mechanical and thermal properties [1]. However, these polymers require hundreds of years to degrade, (ca. >200 years) compared with the short time of use, causing its build-up in landfills and oceans [2,3]. Among many biodegradable polymers as an alternative in replacing conventional polymers, poly (lactic acid) (PLA) is one of the most promising materials. PLA derives from sustainable raw materials such as corn, beets, and wheat, presenting attractive properties such as good biodegradability, low toxicity, easy processability, transparency, and being environmentally friendly [4,5]. PLA is the primary candidate for food packaging due to its biocompatibility, excellent transparency, and exceptional degradability. However, this polymer has disadvantages for packaging, such as high production cost compared with petroleum-derived conventional polymers [6,7], low barrier properties, poor temperature resistance, and brittleness. Due to permeability issues, PLA is considered inferior to polyethylene terephthalate (PET) for long-term food storage applications [6,7].

Abbreviations: PLA, poly (lactic acid); PET, polyethylene terephthalate; LDPE, Low density polyethylene; TEM, Transmission Electron Microscopy; Tg, Glass transition temperature; T_m, Melting temperature.

* Corresponding authors.
E-mail addresses: viviana.moreno@usach.cl (V. Moreno-Serna), paula.zapata@usach.cl (P.A. Zapata).

https://doi.org/10.1016/j.polymdegradstab.2022.109865
0141-3910/

A possible solution has been incorporating nanometric particles into PLA to obtain a nanocomposite material [8–12]. In addition, organic and inorganic nanoparticles have been considered reinforcing agents in the PLA matrix to improve its thermo-mechanical properties [13–15]. The main advantage of nanoparticles is the high specific surface that provides a larger contact area between the particle and the polymer matrix [16].

Metal oxide nanoparticles such as silver (Ag_2O), copper (CuO), or photoactive oxides, such as titanium dioxide (TiO_2) and ZnO with antimicrobial activity, are usually considered feasible alternatives to avoid growth and reducing microorganisms' adhesion in the PLA [4,17].

For example, Fonseca et al. reported obtaining PLA with 5 and 8 wt.% of TiO_2 (10 nm) by a melting process. The elastic modulus of PLA/TiO_2 nanocomposites increased ~54% compared to processed PLA, and this can be related to the excellent distribution of the nanoparticles into the PLA matrix. Besides, nanocomposites showed a reduction of 94.3 and 99.9% against *E. coli* bacteria and *Aspergillus fumigatus* fungus, respectively [4]. ZnO particles (0–5 wt.%, 100–500 nm) were incorporated into a PLA matrix by a melt-mixing extrusion process. Composites loaded with 5 wt.% of ZnO reduced 99% of colony-forming units of *E. coli*. Regarding the mechanical properties, Young modulus increased ca. 11% with ZnO content, and the oxygen permeability decreased by incorporating 1 wt.% of ZnO [18]. Nevertheless, the toxicity of silver nanoparticles is still under evaluation, and TiO_2 and ZnO require UV irradiation for activation, making them unattractive for industrial applications [19–21]. In contrast, calcium oxide (CaO) nanoparticles have received scientific attention due to their high basicity, non-corrosive, recyclable, low-cost bactericidal, and ease of process [22,23]. They are also generally regarded as safe materials, having low toxicity and high biocompatibility [24,25]. Several studies have demonstrated their effectiveness in eliminating natural pathogens such as *E. coli*, *Salmonella typhimurium, Staphylococcus aureus*, and *Bacillus subtilis* [26–28].

The incorporation of CaO nanoparticles into the polymer matrix has been much less studied than in other systems. The antimicrobial properties of the nanocomposites have not been evaluated either [29]. Previously, our research group demonstrated antimicrobial properties for LDPE/CaO nanocomposites (sizes of CaO from 55 nm and 25 nm). The nanoparticles were modified with oleic acid (Ol-CaO), and the CaO and Ol-CaO nanoparticles in different amounts (3, 5, and 10 wt.%) were incorporated into the LDPE by the melting process. Ol-CaO nanoparticles of 25 nm acted as nucleating agents, increasing the polymer's crystallinity. The Young's Modulus of PLA/Ol-CaO increased ca. 36%, regardless of the nanoparticle size, in comparison with the neat PLA. With increased nanoparticle amounts at 10 wt.% and a decrease in size, the reduction in *E. coli* bacteria increased. Besides, the highest antimicrobial behavior was found in the composites with a Ol-CaO of 25 nm, presenting a decrease of 99.9% [30]. Therefore, CaO nanoparticles are considered bactericidal materials with great potential in food packaging or medical devices.

There are few studies of CaO nanoparticles incorporated into PLA. Liu et al. modified calcium oxide (CaO) with n-octadecyl trichlorosilane (CaO-M), and the nanoparticles with and without modification were incorporated into PLA by melt-blend to prepare PLA/CaO and PLA/CaO-M (0–1 wt.%) nanocomposites. CaO-M nanoparticles in the PLA inhibited the cold crystallization of PLA and blocked recrystallization during the second heating process, thus facilitating heterogeneous nucleation. As a result, the PLA/CaO-M (with 0.1 wt.%) increased the degree of crystallinity fivefold compared to that of neat PLA. The tensile strength and impact strength of the PLA/CaO-M nanocomposite material reached their maximum value when the CaO-M content was 0.1% by ca. 32% and 243% higher than neat PLA, respectively [31]. Although the previous reports have studied the manufacturing of polymeric nanocomposites with CaO incorporation, they did not report the antimicrobial properties [30].

In this study, the calcium oxide (CaO) nanoparticle surface was modified with oleic acid to obtain modified calcium oxide (Ol-CaO) in order to improve the interaction between the nanoparticles and the polymer. Then, PLA/CaO nanocomposite films were obtained by varying the loading of CaO and Ol-CaO nanoparticles (5 and 8 wt.%) using a melt blending method. First, the study of thermal and microhardness properties of nanocomposites was performed. Then, the biocidal properties of nanocomposites films were evaluated against *E. coli* bacteria. Finally, the effect of the addition of nanoparticles (CaO) on the photodegradation of PLA was also studied. These biodegradable nanocomposites with antimicrobial properties will allow for future advances in sustainable antimicrobial materials for the medical or food packaging fields.

2. Materials and methods

2.1. Materials

Calcium nitrate tetrahydrate ($CaNO_3)_2{\cdot}4H_2O$, 99%) and oleic acid (90%, technical grade) were purchased from Sigma–Aldrich. Sodium hydroxide (pellets) was obtained from Mallinckrodt Chemicals, USA. Ethylene glycol (99.5%) and chloroform (Emsure®, analytical reagent) were obtained from Merck, Germany. Nitrogen (99.95%, extra pure degree) was obtained from AGA S.A., Chile; ethanol (99.85%) was obtained from Equilab, Chile, and hexane (99.8%) was purchased from J.T. Baker, USA. The pellets of poly (lactic acid) (PLA) were purchased from Oxiqum S.A., Chile, with a density of 1.24 g/cm^3 and 4% content of D-isomer.

2.2. Synthesis of CaO nanoparticles

Calcium oxide (CaO) nanoparticles were prepared by calcination of calcium hydroxide ($Ca(OH)_2$), previously synthesized under assisted sonication [30,32]. As the first step, a solution of $Ca(NO_3)_2{\cdot}4H_2O$ (2.0 M in ethylene glycol) was prepared and placed under sonication for 10 min. Then, the second solution of NaOH (4.2 M in distilled water) was added by dripping to the first solution. The resulting solution was sonicated for 5 min and left to stand for 5 h. The precipitate was then separated by vacuum filtration with distilled water and dried for 24 h at 60 °C. Finally, CaO nanoparticles were obtained by calcination at 500 °C for 5 h.

2.3. Surface-modification of CaO nanoparticles (Ol-CaO)

CaO nanoparticle modifications were made as reported in a previous work by Li and Zhu [33] and our research group [30,34,35]. n-Hexane (50 mL) and oleic acid (800 μL) were added to 1.0 g of CaO nanoparticles. The resulting suspension was placed under sonication for 20 min to improve homogenization. Next, the solution was kept under a nitrogen atmosphere with vigorous stirring for 5 h at 60 °C. Finally, CaO modified (Ol-CaO) nanoparticles were filtered, washed with ethanol, and dried for 24 h in an oven at 60 °C.

2.4. Characterization of CaO nanoparticles

The morphology and size of CaO nanoparticles were obtained through Transmission Electron Microscopy (TEM) using a Philips Tecnai 12 (The Netherlands) microscope at 80 kV. First, the CaO nanoparticles were sonicated for 1 h in ethanol. Then, a drop of CaO-solution was put on a carbon-coated standard copper grid previously sonicated for 20 min, waiting for the solvent evaporation to complete the preparation. Finally, samples of ultrafine

PLA/CaO and PLA/Ol-CaO nanocomposites, with a ca. 100 nm thickness were cut with diamond blades in an ultramicrotome Sorvall MT 5000.

The crystallographic structure of CaO nanoparticles was analyzed using an X-ray diffractometer. The crystalline phase study was carried out in a Siemens D5000 diffractometer, using $0° < \theta° < 80°$ scanning.

The characteristic bands of synthesized and modified CaO were analyzed by Fourier Transform Infrared (FTIR) spectroscopy in a Bruker 22 FTIR spectrometer using a pellet containing a mixture of nanoparticles with KBr. All spectra were obtained in a range of the infrared spectrum with wavelengths between 4000 and 500 cm^{-1}, with a resolution of 4 cm^{-1}.

2.5. Preparation of PLA/CaO and PLA/Ol-CaO nanocomposites films

Previously, the PLA was dried at 60 °C during 24 h before the melting process. Concentrations of 5 and 8 wt.% CaO and Ol-CaO nanoparticles were incorporated into the PLA polymer matrix by the melting process using a Brabender Plasti-Corder internal mixer at 200 °C and 110 rpm for 5 min. Predetermined amounts of the nanoparticles and neat polymer were incorporated to obtain nanocomposites with 5 and 8 wt.% of nanoparticles. Films were molded from nanocomposites using a hydraulic press (Scientific, LabTech Engineering) with heated plates at 180 °C and 50 bar pressures, equipped with a cooling system by potable water circulation. The films were kept at rest during 1 month for aging not to affect the properties.

2.6. Characterization of PLA, PLA/CaO, and PLA/Ol-CaO nanocomposites

The glass transition temperature (T_g), melting temperature (T_m), melting enthalpy (ΔH_m), cold crystallization temperature (T_{cc}), and cold crystallization enthalpy (ΔH_{cc}) were measured on a Mettler Toledo DSC-1 start system. The samples were heated from 25 to 200 °C, at a rate of 10 °C·min^{-1}, and then cooled to 25 °C and heated again at the same rate (10 °C. min^{-1}). The thermograms and values were taken from the second heating scan to avoid the contribution of the thermal history. The percentage of crystallinity was calculated using Eq. (1), using the melting enthalpy of an ideal PLA with 100% crystallinity (ΔH^0_m) by integrating the DSC curve from around 70 to 180 °C [4].

$$X_c = \frac{(\Delta H_m - \Delta H_{cc}) * 100}{\Delta H^0_m \ (1 - x)} \quad (1)$$

Where ΔH^o_m is 93 ($J \cdot g^{-1}$), the enthalpy of fusion of an ideal PLA with 100% crystallinity [4], ΔH_m and ΔH_{cc} are the melting enthalpy and cold crystallization enthalpy ($J \cdot g^{-1}$) of the polymer nanocomposite, respectively, and x is the percent of nanoparticles in the polymer matrix [36].

The thermal stability was evaluated through thermogravimetric analysis (TGA) using a TGA/SDTA 851 Mettler-Toledo setup under Argon inert atmosphere (50 mL·min-^{1}). Samples in triplicates were introduced into alumina crucibles and heated from 25 to 600 ° C at a heating rate of 10 °C·min^{-1}. The TGA analysis has a standard deviation of ca. ± 2 °C.

The Microhardness (MH) of neat PLA and PLA/CaO and PLA/Ol-CaO composites were measured in and Vickers hardness, Leitz Miniload 2 device at 29 °C under a charge of 0.981 N and an application time of the charge of 25 s.

2.7. Antimicrobial properties of PLA/CaO nanocomposites

The antimicrobial effect of the different samples was determined using a plate count method described in the ISO 20,743.41 *E. coli* ATCCC 25,922 was used as microbes for analysis [30,37]. In brief, the initial number of bacteria present after incubation was calculated by counting the number of colonies in a ten-fold dilution. A microbial suspension of 1×10^7 CFU·mL^{-1} (CFU: colony forming units) by Densimat bioMérieux® was prepared in a BHI broth plus Triton 100x in a humid chamber. 0.5 mL of the suspension was placed in contact with every 2.5 cm^2 sample. Control and antibacterial-treated samples were recovered by suspension in 10 mL of sterile saline solution and then serially diluted down to 1/10, 1/100, and 1/1000. Then, 0.2 mL of each dilution was plated in duplicate on trypticase soy agar plates and incubated at 37 °C for 24 h under UV and white light. After incubation, the number of colonies in the Petri dishes was counted, and the percentage of inhibition was determined compared to its corresponding control. The percentage of colony reduction was calculated using Eq. (2), which relates the number of colonies of the neat polymer to the number of colonies from the nanocomposites (PLA/CaO and PLA/Ol-CaO).

$$\%\ Reduction = \frac{CFU_{neat\ \ polymer} - CFU_{nanocomposite}}{CFU_{neat\ \ polymer}}\ x\ 100 \quad (2)$$

2.8. Photodegradation properties of PLA/CaO nanocomposites

Films generated from neat PLA, PLA/CaO, and PLA/Ol-CaO, with 5 and 8 wt.% of nanoparticles, with 0.1 mm of thickness were put in the camera and irradiated using a Suntest/Atlas XLS oven 2200 W with a standard solar filter (borosilicate), which provides irradiation of 550 $W \cdot m^{-2}$ (Irradiation acc. to ISO 4892/DIN 53,387) in the 300 to 800 nm wavelength region. Previous studies of Therias et al. [38] and Gardette et al. [39] concerning the photo-oxidation mechanism of neat PLA have demonstrated that PLA can directly absorb light in the range of 300 nm and PLA can be sensitive to photo-oxidation with wavelengths greater than 300 nm, promote the chains scission and therefor its degradation [38,39]. The temperature was kept constant at 45 °C during the test. Monitoring was done by taking samples every 24 h for five days.

Viscosimetric analysis before and after irradiation was measured in chloroform at 25 °C in an Ostwald viscometer. The viscosity average molecular weight ($\bar{M}_v$) values of the polymer were obtained from the Mark-Kuhn-Houwink (Eq. (3)), and the constants K and a were 5.46×10^{-4} dL·g^{-1} and 0.7, respectively.

$$[\eta] = K * \bar{M}_v^a \quad (3)$$

Where $[\eta]$ is the intrinsic viscosity, K and a are constants, values of which depend on the nature of the polymer, solvent, and temperature.

Before and after irradiation of nanocomposite films, the morphological analysis was analyzed using a scanning electron microscope (SEM) Hitachi TM 3000. The samples are previously coated with a thin layer of gold to give them a conductive character.

3. Results and discussion

3.1. CaO and Ol-CaO nanoparticles characterization

The CaO nanoparticles were obtained as a fine white powder with a 56% weight yield. The TEM image is displayed in Fig. 1**.** It shows that the nanoparticles presented a spherical shape with an average diameter of 26.1 ± 3.3 nm.

Fig. 2 displays the crystalline structures of the CaO nanoparticles. The XRD pattern of the CaO showed different diffraction peaks in a 10°– 80° range, which coincides with those reported by other authors [22,40–42]. CaO nanoparticles exhibited diffraction peaks (2θ) at 36°, 64°, and 65°, which are assigned to the (200), (311), and (222) planes of the cubic structure of CaO, respectively. Other

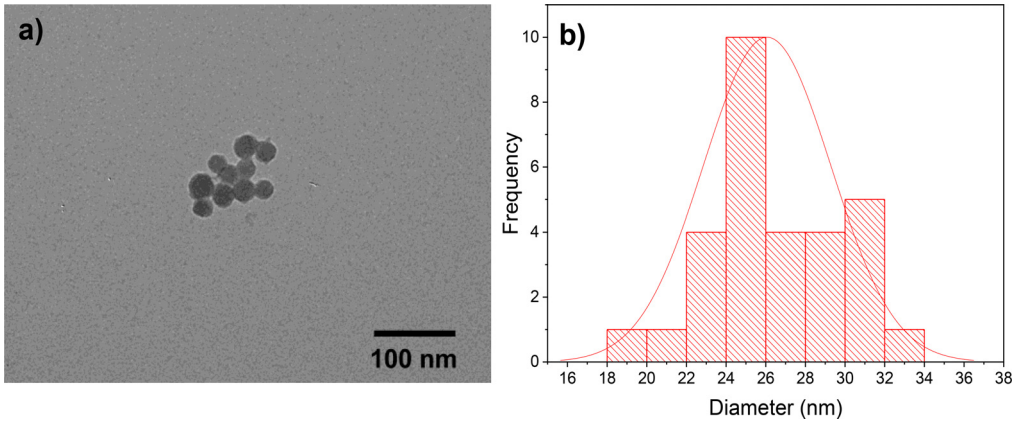

Fig. 1. a) TEM image and b) histogram of CaO nanoparticles.

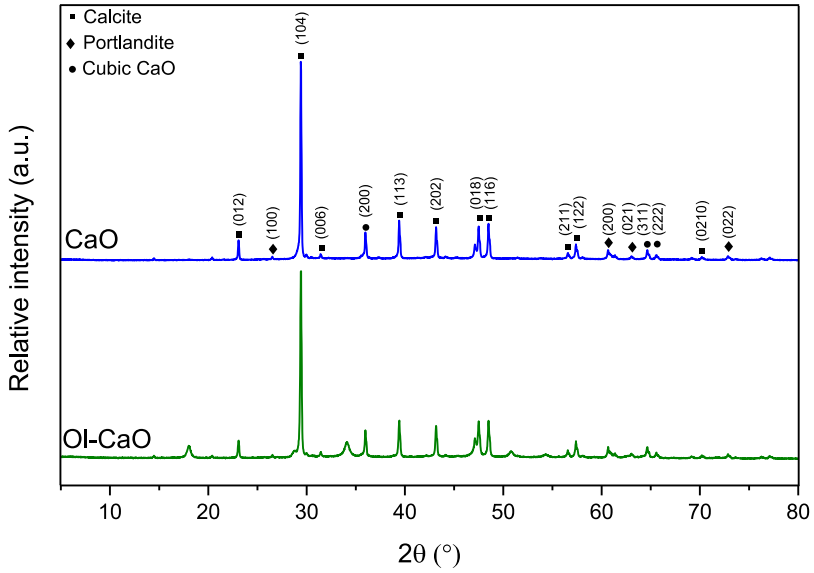

Fig. 2. XRD pattern of CaO and Ol-CaO nanoparticles.

diffractions peaks (2θ) at 23°, 29°, 31°, 39°, 43°, 47°, 48°, 56°, 57°, and 70°, associated with the (012), (104), (006), (113), (202), (018), (116), (211), (122), and (0210) planes correspond to calcite phase of CaO, respectively. Finally, the presence of peaks (2θ) at 26°, 61°, 63°, and 73°, attributed to (100), (200), (021), and (022) plans reveal the structure of portlandite phase $Ca(OH)_2$ [22,40–42]. In contrast, upon modification of the CaO nanoparticles, the main XRD peaks were kept, suggesting that chemisorption with oleic acid would not alter the domains and crystalline phases of the metal oxide nanoparticles [43,44].

FTIR analysis was conducted on pure oleic acid (OA), CaO, and Ol-CaO (Fig. 3**)** to examine the characteristic peaks of the nanoparticles**.** The CaO FTIR spectrum shows an absorption peak at 3642 cm^{-1} resulting from the O–H bond from water molecules on the surface of nanoparticles [22,45,46]. There is a tiny dip in the spectra at 2359 cm^{-1} due to the presence of atmospheric CO_2. A band around 550 cm^{-1} identified the vibration of Ca–O bonds, while the broadband at 1446 cm^{-1} and a strong band around 875 cm^{-1} indicate the C–O bond related to CaO nanoparticles carbonation [47]. On the other hand, the spectrum of Ol-CaO shows that the nanoparticles were modified after treatment with oleic acid, as suggested by the signals associated with the vibration at 2923 and 2854 cm^{-1}, assigned to C–H stretching modes of the oleic acid alkyl chain. Three high-intensity peaks should appear in the range 1650–1360 cm^{-1} as a double and a single peaks assigned to the asymmetric and symmetric C–O stretching vibrational modes of carboxylate groups [48]. Interaction via acid-base chemisorption between the fatty acid adsorbate, oleic acid, and hydroxyl groups from the basic CaO surface, $Ca(OH)_2$ (portlandite phase, see Fig. 2), produces calcium oleate salt. It is constituted by carboxylate ($RCOO^-$) and Ca^{2+} ions [49,50]:

$$Ca(OH)_2 + 2RCOOH \leftrightarrow (RCOO)_2Ca + 2H_2O$$

R: $CH_3(CH_2)_7CH{=}CH(CH_2)_2CH_2$-

Moreover, the weak band at ca. 1450 cm^{-1} assigned to the bending of -CH_2- groups of calcium oleate aliphatic chain is not observed. As a result, carboxylate and -CH_2- bending peaks are overlapped with the broad and intense CaO characteristic peak at 1490 cm^{-1} [51].

In the FTIR spectra of the organically modified nanoparticles, the peak intensity of the O–H stretching vibration decreased ca. 40% compared to neat CaO nanoparticles due to the reaction of the carboxyl group in oleic acid with the hydroxyl group of CaO portlandite phase [33]. These results agree with the metal oxide nanoparticles coating with oleic acid chemisorbed between carboxylate groups as adsorbate and nanoparticle surface [52–54].

Thermogravimetric analysis (TGA) of neat CaO nanoparticles (Fig. 4) showed a decomposition temperature at 10% weight loss

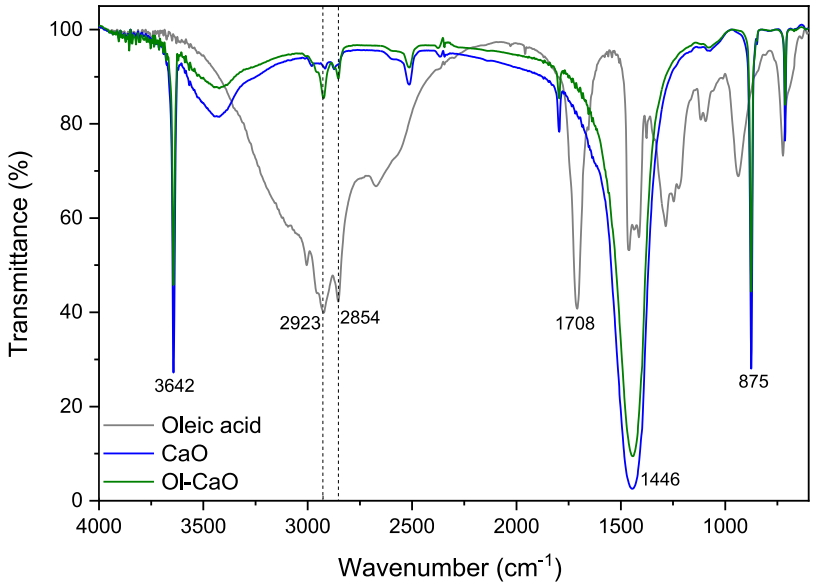

Fig. 3. FTIR spectrum of oleic acid (OA), CaO nanoparticles, and CaO modified nanoparticles with oleic acid (Ol-CaO).

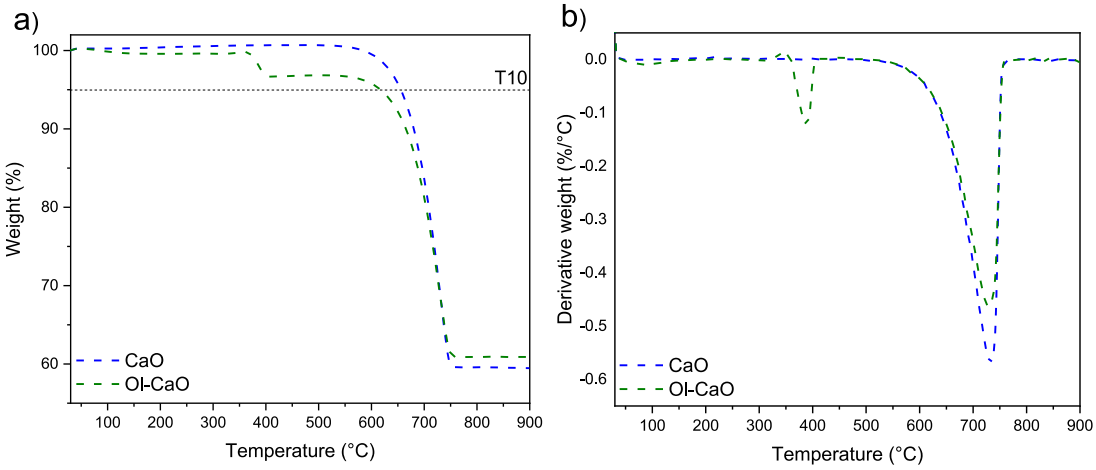

Fig. 4. a) TGA and b) differential thermogravimetric (DTG) curves of CaO and Ol-CaO nanoparticles.

(T_{10}) of 656 °C, while Ol-CaO nanoparticles showed a decrease in the T_{10} compared to CaO nanoparticles at 619 °C due to oleic acid chemisorption. Moreover, Ol-CaO nanoparticles exhibited a weight loss of ca. 4% up to 360 °C, corresponding to decomposition of oleic acid. The differential thermogravimetric (DTG) curve of Ol-CaO nanoparticles exhibited two peaks; the first is at 388 °C due to the presence of the oleic acid in the nanoparticles, confirming the acid-base chemisorption between oleate chains and Ca^{2+} on the nanoparticle surface. The temperature for maximum weight loss rate (T_{max}) of neat and modified nanoparticles in the DTG curves does not change notoriously (ca. 730 °C). Previous studies have reported similar oleic acid content and chemisorption for Fe_3O_4 [55], and TiO_2 [56] metal oxide nanoparticles.

3.2. Characterization of PLA/CaO and PLA/Ol-CaO nanocomposites

3.2.1. Dispersion and thermal analysis

The dispersion of the CaO and Ol-CaO (5 and 8 wt.%) nanoparticles into the PLA matrix were analyzed by Transmission Electron Microscopy (TEM), as displayed in Fig. 5. The nanocomposites with unmodified nanoparticles exhibit low dispersion due to nanoparticle agglomeration. In the case of modified nanoparticles (Ol-CaO), a better distribution was observed. The CaO nanoparticles showed low dispersion in hydrophobic polymer matrices, while the nanoparticles modification added hydrophobic domains on the surface of the Ol-CaO nanoparticles [33,54]. PLA is a hydrophobic polymer, and hydrophobic interaction between PLA and the oleic acid layer of the CaO surface nanoparticles occurs, such as London dispersion interactions, which improved nanoparticle dispersion within nanocomposites [57]. On the other hand, the carboxyl group in oleic acid could react with active groups on the surface of nanoparticles as a hydroxyl group. The long alkyl chain and unsaturated bond in oleic acid provide significant hydrophobicity to the nanoparticles and benefit good interfacial bonding between the nanoparticles and the polymer matrix. As a result, the nanoparticles modified by oleic acid can prevent their aggregation and enhance the dispersion into the polymer [57].

The thermal properties were assessed using differential scanning calorimetry (DSC) (Fig. 6). Table 1 displays the results of thermal properties as glass transition (T_g), cold crystallization temperature (T_{cc}), melting temperature (T_{m1} and T_{m2}), and percent crystallinity (X_c) of neat PLA, PLA/CaO, and PLA/Ol-CaO nanocomposites obtained from the second heating.

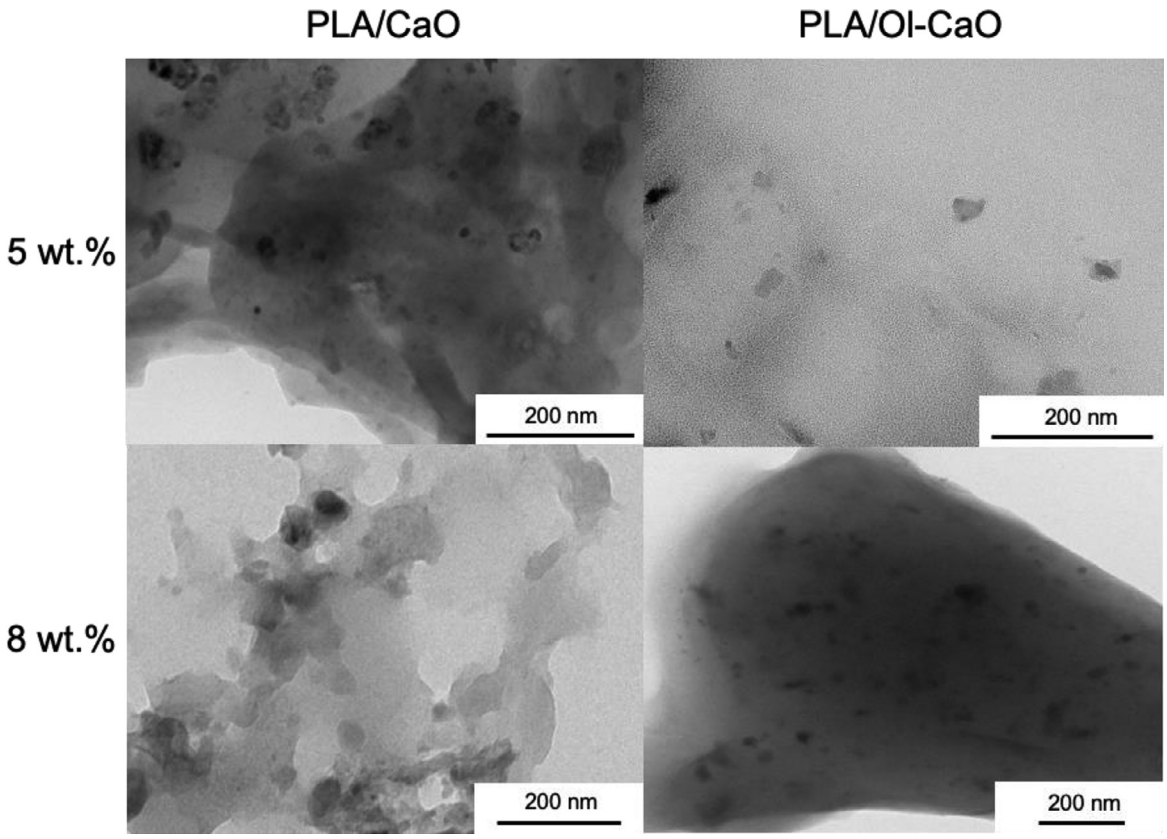

Fig. 5. TEM images of PLA/CaO nanocomposites with 5 and 8 wt.% of CaO and OI-CaO nanoparticles.

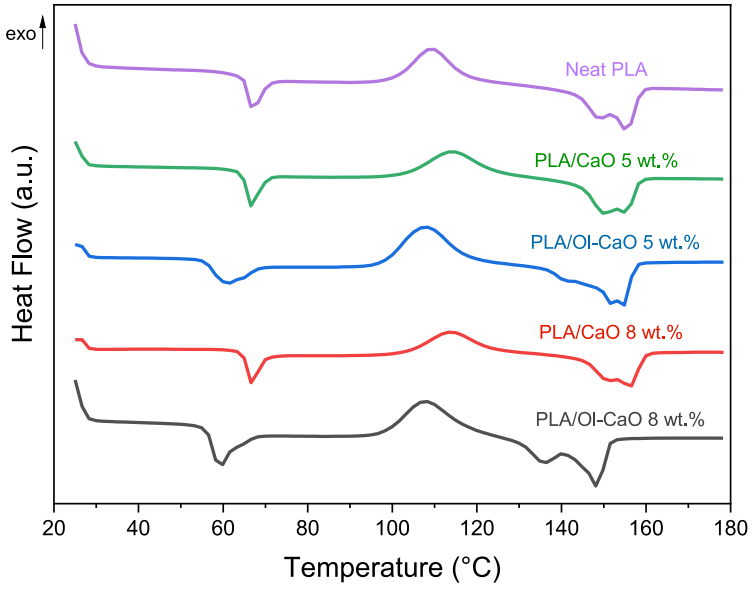

Fig. 6. DSC thermograms of neat PLA, PLA/CaO, and PLA/OI-CaO nanocomposites loaded with nanoparticles at 5 and 8 wt.% of second heating.

Table 1
Thermal properties of neat PLA, PLA/CaO, and PLA/OI-CaO.

Sample	CaO (wt.%)	T_g (°C)	T_{cc} (°C)	T_{m1} (°C)	T_{m2} (°C)	X_c (%)	T_{10} (°C)	T_{max} (°C)
Neat PLA	0	63	110	150	155	1	313	342
PLA/CaO	5	63	113	150	155	1	235	275
	8	63	113	152	157	1	247	264
PLA/OI-CaO	5	55	108	152	155	0	226	279
	8	55	108	137	148	2	229	262

T_g: Glass Transition, T_{cc}: Cold Crystallization Temperature, T_{m1}; T_{m2}: Melting Temperatures and X_c: Crystallinity Percentage, T_{10}: Decomposition Temperature at 10% Weight Loss, T_{max}: Temperature for Maximum Weight Loss Rate.

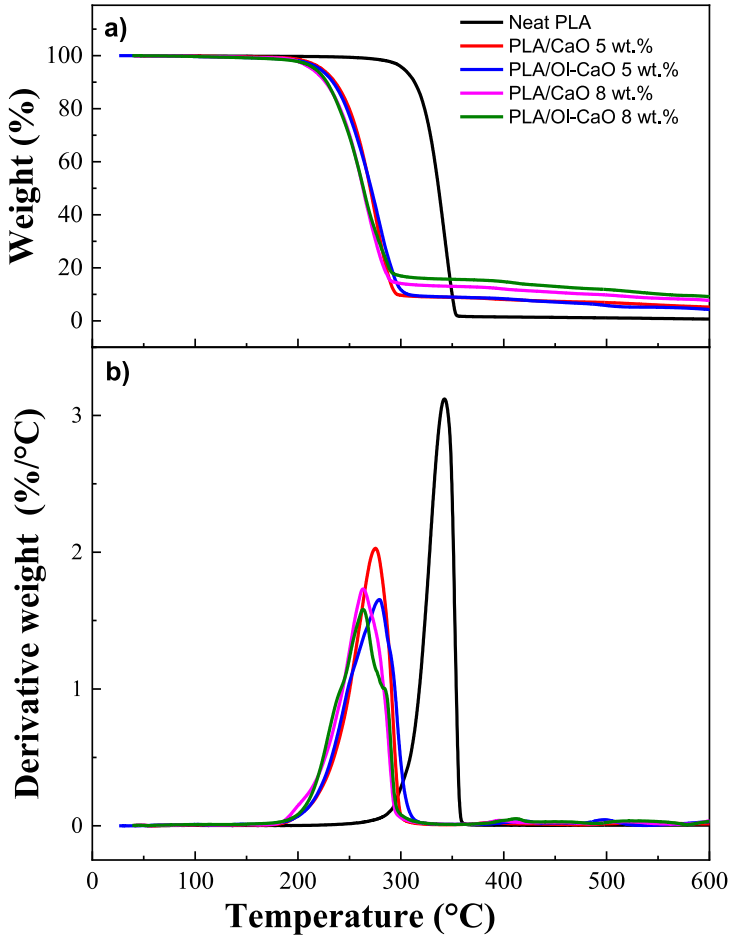

Fig. 7. a) TGA and b) Derivative TGA of neat PLA, PLA/CaO, and PLA/Ol-CaO nanocomposites with nanoparticles at 5 and 8 wt.%.

As expected for semicrystalline PLA, the curves revealed three thermal transitions. First, an endothermic peak was associated to structural relaxation during the glass transition. Then, an exothermic transition was found due to the cold crystallization process. Finally, a melting process for the crystalline domains was found. The appearance of a cold crystallization and subsequent melting peak with a comparable enthalpy denotes the low crystalline character of the samples after processing [58].

The glass transition temperatures of PLA/CaO nanocomposites did not change concerning the neat PLA, while for PLA/Ol-CaO, the decrease was ca. 13%. Similar results were found for PLA/oleic-silica nanocomposites in the literature. A slight decrease in T_g (ca. 3%) was reported for 5 wt.% oleic acid-treated silica-filled PLA nanocomposites [59].

On the other hand, the cold crystallization temperatures (T_{cc}) decrease slightly by incorporating Ol-CaO nanoparticles acting as nucleation agents compared to neat PLA. Similar results were reported by Nofar et al., evidencing that the presence of nanoparticles such as nanosilica (12 nm) and nanoclay (100 nm) in PLA slightly improves its crystallization due to incremented chain mobility [60]. Finally, the nanoparticles dispersion in the polymeric matrix is an essential factor in crystallization. Therefore, the surface modification of CaO enhances its distribution into the macromolecular chains (in PLA/Ol-CaO nanocomposites), which induce the formation of crystals of PLA [61,62].

The melting temperature of neat PLA, PLA/CaO, and PLA/Ol-CaO nanocomposites presented two distinct peaks (T_{m1} and T_{m2}) due to polymorphism of different crystal structures of PLA or lamellar populations with varying degrees of perfection [63]. The low-temperature endothermic process is related to melting meso–stable crystals or less perfect crystal; after this melting process, more stable crystals are formed, explaining the high-temperature endothermic peak [4,64]. Other authors have also reported two peaks in the melting temperature with the incorporation of nanoparticles, attributing the behavior to PLA/nanoparticles due to the formation of two crystal structures with different sizes or perfection of ordering [65,66]. It was observed that for both T_{m1} and T_{m2}, it only decreases slightly for PLA/ Ol-CaO with 8 wt.% compared to the neat PLA. Although nucleating agents are known to generate multiple nuclei with low lamellar thickness, the synergistic performance of oleic acid and nanoparticles in this percentage resulted in a semicrystalline structure with the highest degree of perfection [4,64].

The neat melting enthalpy, considered the sum of melting and crystallization in the range from 70 to 180 °C, is negligible for PLA, highlighting the amorphous structure of this material, obtaining X_c ca. 1% [67]. The presence of nanoparticles did not affect the crystalline fraction of PLA. Similar phenomena were observed in the literature dealing with nanocomposites, processed mainly by melt blending [61,68–71].

On the other hand, TGA studied the effect of the addition of CaO and Ol-CaO nanoparticles on the thermal stability of PLA-based nanocomposites in a nitrogen atmosphere. The TGA and derivative TGA of neat PLA, PLA/CaO, and PLA/Ol-CaO nanocomposites are displayed in Fig. 7, and the results are summarized in Table 1. The neat PLA showed a main peak of T_{max} of 342 °C associated with their thermal degradation [72]. The PLA/CaO and PLA/Ol-CaO nanocomposites decreased in the T_{10} ca. 28% and T_{max} ca. 23% compared to the neat PLA. Thus, the thermal stability of the nanocomposites decreased with the amount of CaO and

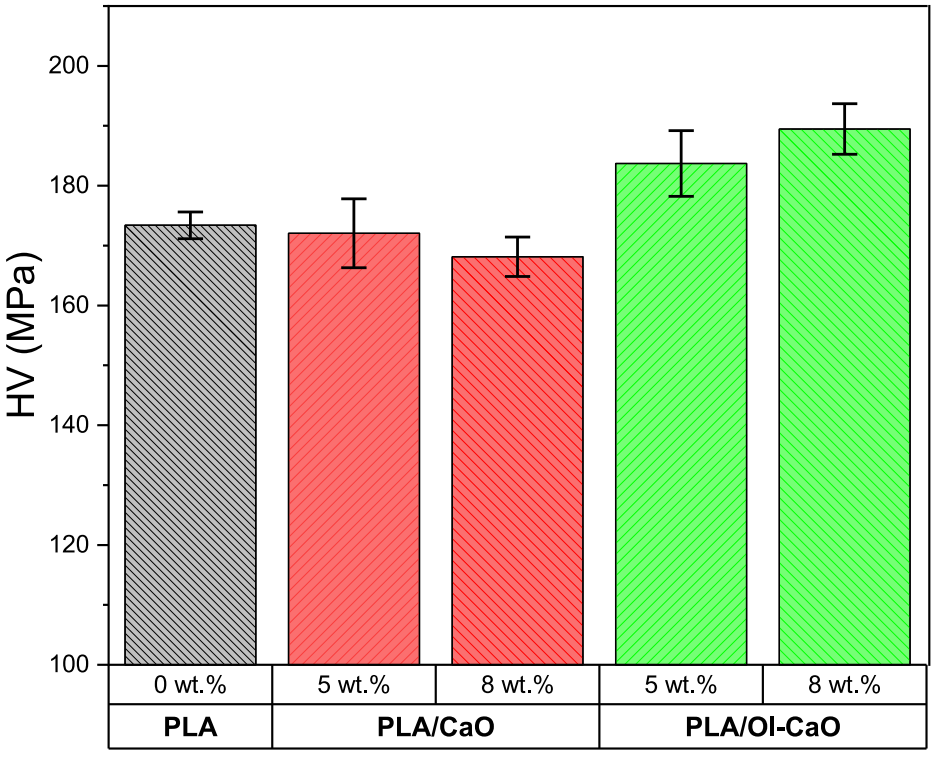

Fig. 8. Vickers Microhardness (HV) of neat PLA, PLA/CaO, and PLA/Ol-CaO nanocomposites.

Ol-CaO nanoparticles incorporation. Similar results were found by Fan et al. for PLLA/CaO nanocomposites. The PLLA was degraded through unzipping depolymerization, occurring in a temperature range of 250–320 °C [73]. The authors reported that chains of PLLA decomposition start with reactions with CaO, followed by a backbiting reaction from chain-end anions. The depolymerization is caused by the attack of the CaO on the PLA ester carbonyl carbon, which leads to the formation of oligomers with carboxylic end groups or calcium carboxylate. Then, the carboxylic ion is attached to the asymmetric carbon atom in the penultimate unit of the PLLA, followed by scission of the C–O bond between methine carbon and ester oxygen [74,75].

Other authors have reported a reduction in the thermal stability of PLA/$CaCO_3$ nanocomposites compared to the neat PLA. These results were attributed to the alkali nature of $CaCO_3$, capable of catalyzing the PLA depolymerization through ester bonds. The basic nature of $CaCO_3$ catalyzed the depolymerization of the PLA ester bonds, reducing the thermal stability [76,77]. In the same way, some metal compounds can also catalyze PLA by pyrolysis, resulting in a decreased degradation temperature [78–80]. For example, it is reported that PLA/ZnO nanocomposites degradation temperature decreased compared to the neat PLA due to catalytic activity of ZnO, leading to polymer thermal degradation at a lower temperature [81]. This degradation is attributed to the fact that zinc compounds catalyze intermolecular transesterification reactions. This reaction generates lower PLA molecular weight and the "unzipping" depolymerization, which leads to selective formation of lactide acid [82].

3.2.2. Microhardness

The mechanical properties were evaluated through microhardness analysis. As the samples of this study were obtained through thermo-compression, in addition to the difficulty of preparing samples of the films without cracks, the evaluation of mechanical properties with a tensile test was discarded. The Vickers Microhardness (HV) of neat PLA, PLA/CaO, and PLA/Ol-CaO nanocomposites are displayed in Fig. 8**.** The PLA/CaO nanocomposites did not show a considerable change in the microhardness of nanocomposite films compared with neat PLA. It has been reported that low dispersion of the nanoparticles could cause a low efficiency in the transmission of efforts made on the matrix towards the nanoparticles, maintaining and even decreasing their mechanical properties [83,84]. On the other hand, PLA/Ol-CaO nanocomposites showed increased microhardness ca. 9% concerning neat PLA, showing the effect of these modified nanoparticles on the microhardness of the PLA polymer matrix. These results can be related to the dispersion of modified-surface CaO nanoparticles into PLA, as confirmed previously by TEM images (Fig. 5**).** The effective transmission of the stress is applied from a matrix to nanoparticles [85,86]. The microhardness and Young's modulus behavior depend on the polymer structure, and therefore they should show the same trend [87,88]. Therefore, it has been reported that microhardness and the elastic modulus are reciprocally dependent, and both are correlated to the polymer structure and composition. [64,87,88]

For example, the authors reported that the good dispersion of the TiO_2 (10 nm) nanoparticles within PLA increased ca. 34% the Young's modulus in comparison with neat PLA [4]. On the other hand, the increased strength indicates good interfacial adhesion between the matrix and the nanoparticles and stress transfer of TiO_2 particles to the polymer [4]. Sallal et al. studied the effect of the Al_2O_3-CaO nanoparticle incorporation into the polymer blend. The authors found that the polymer blend showed an increase ca. 25% in hardness values with the nanoparticle incorporation (2 wt.%). This indicating that the nanoparticles give the polymer matrix high resistance against scratching with a high surface area. Thus it enhances the strength of the interface between the nanoparticles and the polymer [89].

3.2.3. Antimicrobial analysis of PLA/CaO and PLA/Ol-CaO nanocomposites

The antimicrobial properties of PLA/CaO and PLA/Ol-CaO nanocomposites against *E. coli* are given in Table 2. The re-

Table 2
Reduction percentage of *E. coli* bacteria against PLA/CaO and PLA/Ol-CaO nanocomposites.

Sample	CaO (wt.%)	*E. Coli* reduction (%)
PLA/CaO	5	57.1
	8	95.5
PLA/Ol-CaO	5	54.6
	8	99.9

sults found for the antimicrobial activity yielded an error of ca. 3%. As observed, the antimicrobial properties of nanocomposites increased with the nanoparticle concentration and it increased slightly with the nanoparticles modification. Incorporation of the modified nanoparticles reaching ca. 99.9% reduction against *E. coli*. The antimicrobial action of the CaO nanoparticles is expected to depend on the interactions between bacterial cells and CaO. However, the antimicrobial mechanism of the CaO nanoparticles is still unclear [90,91]. It could be due to three possible mechanisms: (1) generation of reactive oxygen species (ROS), which results in oxidative stress in the bacterial cells, (2) disruption of bacterial cell membrane followed by cellular content leakage, and (3) increase in pH value due to CaO hydration in water [28,92].

ROS such as $HO_2^{\cdot}$, O_2^{-}, and H_2O_2 generated from the surface of CaO interact with the constituent carbonyl groups of the bacterial cell wall peptide bond/polyunsaturated phospholipids and influence protein degradation, which consequently leads to the destruction of the bacterial cell wall [93]. Concerning the second mechanism proposed, electrostatic forces between CaO and bacterial cell membranes cause damage to the bacteria cell membrane. On the other hand, the alkaline effect has been considered another primary factor in the antimicrobial action of CaO nanoparticles. The adsorption of water moisture on the CaO nanoparticle surfaces could form a thin layer of water around the particles. The local pH of this thin water layer formed around the nanoparticles could be much higher than its equilibrium value in the solution. When the nanoparticles are in contact with the bacteria, the high pH in this thin surface water layer could damage the membrane, resulting in cell death [28,94]. Therefore, the antimicrobial results may be related to the release of Ca^{2+} ions from the PLA matrix and the mechanism associated with the increase in pH by the hydration of CaO with water, forming hydroxides, and releasing Ca^{2+} ions [95]. Ro et al. state that the biocidal effect may be due to alkalinity, with hydration of CaO as one of the basic antimicrobial mechanisms. A study reported by our group showed that the release of Ca^{2+} ions from a polymeric matrix is related to antimicrobial properties [30]. The results of these studies provide evidence that the antimicrobial activity of CaO is not only affected by ROS production. Regarding the results, the CaO nanoparticles have the potential to be used as a powerful antimicrobial agent for manufacturing safe food and medicinal products.

3.3. Photodegradation analysis of PLA and PLA/CaO nanocomposites

The main purpose of the photodegradation study was to analyze the performance of CaO nanoparticles in the degradation of PLA nanocomposites because the effect of these nanoparticles has not been studied in the literature; therefore, only nanocomposites with unmodified CaO were used in this research.

The neat PLA and PLA/CaO nanocomposites were photoaged for five days under irradiation in a wavelength range of 300 to 800 nm. Previous studies concerning the photo-oxidation mechanism of neat PLA have demonstrated that PLA can directly absorb light starting at 300 nm and is sensitive to photo-oxidation with wavelengths greater than 300 nm, causing cleavage or scission of

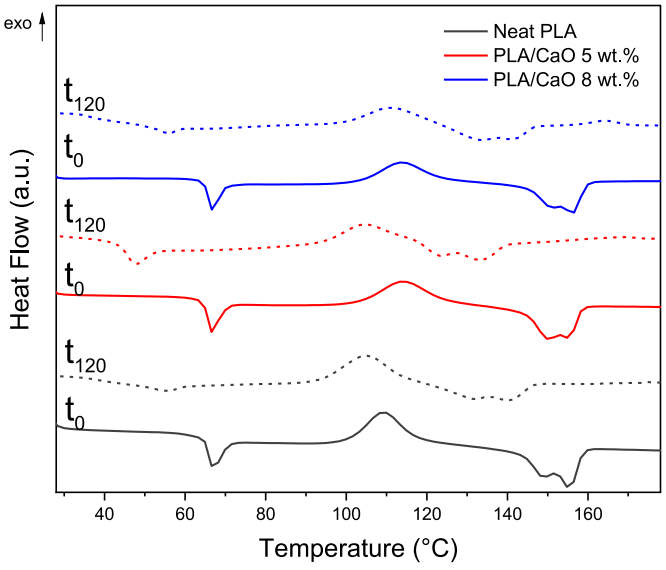

Fig. 9. DSC thermograms of neat PLA and PLA/CaO nanocomposites with 5 and 8 wt% of the nanoparticles before (t_0) and after (t_{120}) irradiations.

chains and resulting in the formation of several photoproducts. The main products that have been detected during the analysis of the solid PLA films are macromolecular anhydrides, or those coming from the C – C bond homolysis on the macromolecular chain, scission of the C–CH_3 bond, would produce a methyl radical CH_3 that can be oxidized to give methanol [38,39,96].

The glass temperature (T_g), crystallization temperature (T_{cc}), melting temperature (T_m), and degree of crystallinity (X_c) were obtained by DSC (Fig. 9), and viscosimetric molecular weight (M_v) of the PLA and PLA/CaO nanocomposites before and after irradiation were displayed in Table 3. The T_g of PLA and PLA/CaO nanocomposites decreased after 120 h of irradiation and was more pronounced for the nanocomposites; this effect is evidence of the photodegradation of polymers [97]. Similar results were reported by K. Fukushima et al., who explained that for PLA/clay nanocomposites, the increased mobility of the polymer chains was due to a plasticizing effect of lactic acid oligomers formed during degradation [63]. After photoaging, nanocomposites' T_{m1} and T_{m2} temperatures also decreased slightly (ca. 7% and ca. 5%, respectively) compared to neat PLA. This is because, during the photodegradation process, the secondary links of the polymer chains are broken, allowing greater mobility of the chains and reducing the energy required to reach the glass state and the melting transition [98,99].

As is observed in Table 3, the irradiated samples, compared with starting samples, exhibit a crystallization region shifted to lower temperatures, while the crystallinity percentage increased in all cases (ca. 7%). The depression of crystallization temperature in the nanocomposites is probably induced by the nanoparticles [67,100,101]. Pan et al. related the change of T_{cc} in PLA due to a decreasing molecular weight peak, indicating that the crystallization rate increased with decreasing molecular weight [102]. Authors have explained the increase in the crystallinity percentage, arguing that during photodegradation, the sample suffers annealing, enabling the polymer chains in the amorphous region to form new ordered domains and favoring the formation of tiny and more perfect crystals, causing increased crystallinity [103,104]. Thus, the changes in the crystallinity of the polymer matrix during degradation can be associated with two phenomena: 1) annealing, allowing the formation of new crystals or increasing their size, and 2) oxidation followed by chain scission in the amorphous region, facilitating crystallization of released chains [35,98]. Furthermore,

Table 3
Thermal properties and viscosity molecular weight ($\bar{M}$**v**) as a function of time of radiation exposure.

Sample	Exposure time (h)	T_g (°C)	T_{cc} (°C)	T_{m1} (°C)	T_{m2} (°C)	X_c (%)	η (dL/g)	$\bar{M}$v (g/mol)
Neat PLA	0	63	110	150	155	1	1.39	73,510
	120	55	105	132	140	8	0.25	6,430
PLA/CaO 5 wt.%	0	63	113	150	155	1	0.86	36,760
	120	48	105	123	133	6	0.09	1,350
PLA/CaO 8 wt.%	0	63	113	152	157	1	0.85	36,090
	120	57	111	133	140	6	0.07	1,010

T_g: Glass transition temperature, T_{cc}: Cold crystallization temperature, T_{m1}; T_{m2}: Melting temperatures, X_c: Crystallinity percentage, η: intrinsic viscosity and $\bar{M}$v: viscosity molecular weight.

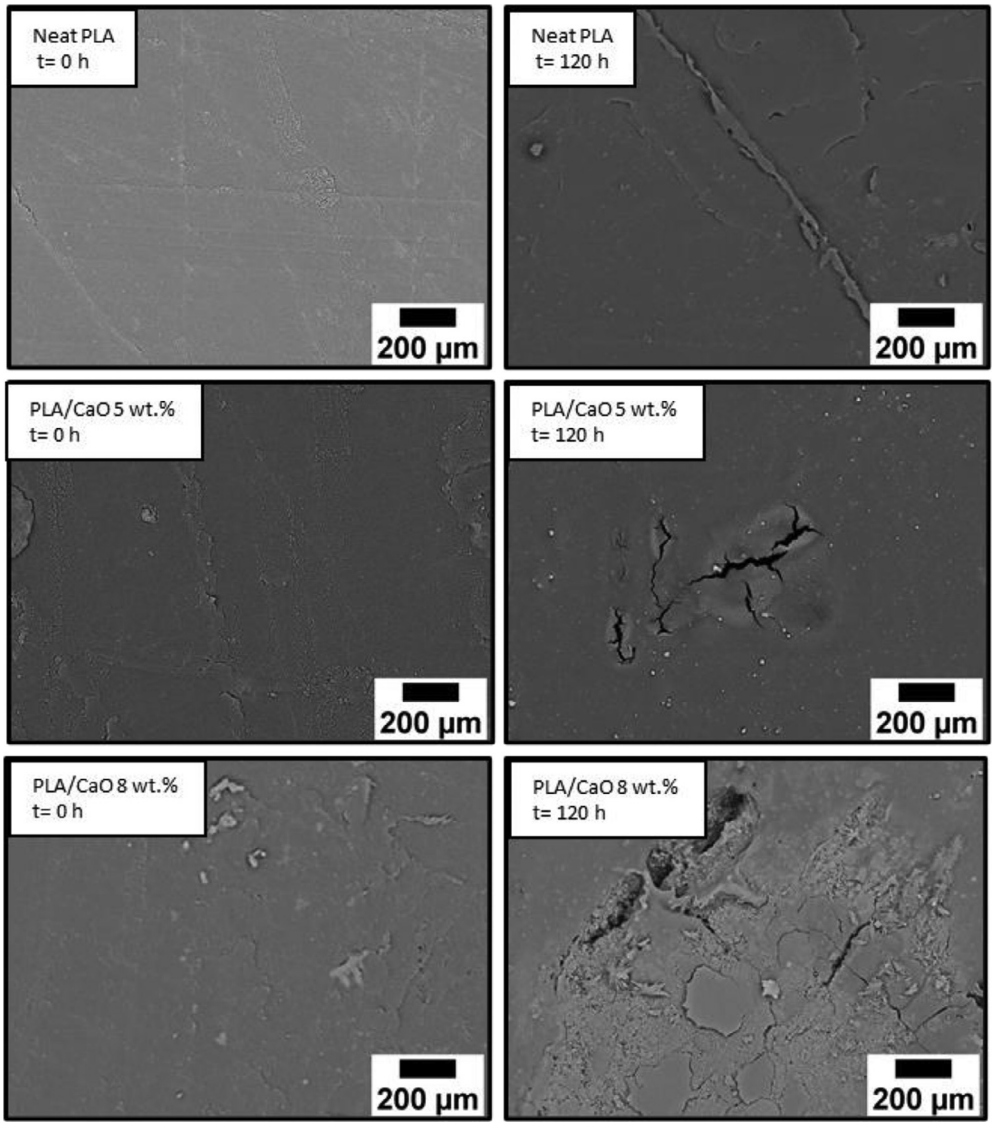

Fig. 10. SEM images before and after 120 h exposure to photodegradation of neat PLA and PLA nanocomposites loaded with CaO at 5 and 8 wt.%.

the scission of the polymer molecule in the amorphous domain during aging leads to the formation of low molecular segments, evidenced in the decrease of the molecular weight of the polymers [105].

The viscosity molecular weight ($\bar{M}$v) of PLA/CaO without irradiation decreased ca. 50% compared to the neat PLA before irradiation. Similar results have been explained due to a slight degradation of the PLA, which can be attributed to a thermo-mechanical and hydrolysis reaction under the melt processing conditions [106,107]. For PLA/organo-modified montmorillonite, Chavéz-Montes et al. also reported a decrease in molecular weight compared to the neat PLA [106]. Fukushima et al. reported that the PLA/clay nanocomposites reduced molecular weight compared to the neat PLA during the melting process due to hydroxyl groups favoring alcoholysis reactions. This fact could explain the higher losses of molecular weights observed for the nanocomposites than the unfilled PLA, given the presence of –OH groups in the organic clay modifiers and on the clay platelet surfaces [63].

The depolymerization caused by the attack of the CaO nanoparticles on PLA before irradiation can also be verified by the de-

creasing in the thermal stability with the incorporation of CaO and O–CaO nanoparticles, as observed previously by TGA analysis, which is accelerated with increasing temperature.

The viscosity average molecular weight ($\bar{M}v$) of PLA and PLA/CaO nanocomposites decreased ca. 91 and 97% after photodegradation, respectively. Incorporating CaO nanoparticles into the polymer promoted or accelerated the PLA degradation, which is a consequence of the catalytic activity of CaO [99,108]. Li et al. explained that the polypropylene/$CaCO_3$ composites showed a higher degradation rate than neat polypropylene due to hydroxyl groups on the surface of nanoparticles catalyzed the photooxidant reaction of polypropylene. Therefore, the hydrophilic surface of nanoparticles is responsible for the increased degradation of the polymer matrix [109]. Previously, our group also confirmed the scission of low-density polyethylene (LDPE) of LDPE/$CaCO_3$ nanocomposites after photoaging, finding that the viscosity decreased due to the formation of low molecular weight compounds during aging. It was noted that this behavior is slightly greater for nanocomposites than for neat LDPE. These results show that the incorporation of nanoparticles into the polymer accelerates its degradation [110].

Fig. 10 shows the SEM micrographs taken of the sample surface of neat PLA nanocomposites and PLA loaded nanoparticles at 5 and 8 wt.% before and after irradiation for 120 h. Non-irradiated PLA and PLA/CaO nanocomposite films showed a smooth and homogeneous surface morphology. After irradiation, the morphology of all nanocomposites changed notoriously. Some cavities and cracks were formed due to surface deterioration caused by irradiation, compared to neat PLA. It is induced by escaping volatile compounds (as CO_2, methane, acetaldehyde, among others) from the PLA matrix related to hydrolysis degradation [98,111,112]. Degradation increases with the content of nanoparticles, and with the incorporation of 8 wt.% of nanoparticles, there was a certain degree of material detachment. The results confirmed that incorporating CaO nanoparticles promotes the deterioration of films when exposed to radiation due to CaO catalytic activity reported [113,114]. Previous reports show that nanoscale incorporation of particles in polymeric matrices leads to greater photodegradation than the neat polymer [115–117]. The mechanism of the photooxidation of PLA has been reported [117,118]. A classical hydrogen abstraction explains this on the polymeric backbone at the tertiary carbon in the α-position of the ester function, resulting in alkyl macroradicals. These macroradicals react with oxygen, resulting in peroxy radicals that produce hydroperoxides. Once formed, hydroperoxides can decompose, leading to the formation of alkoxyl and hydroxyl radicals propagating the chain reaction by hydrogen abstraction from the polymer backbone or undergo β-scission. Macroradicals consisting of alcohol and ketone groups are also generated and subsequently oxidized. Carboxylic acids and carbonylated derivatives are produced by the scission of the macroradical backbones [117,118].

Nevertheless, the PLA photodegradation mechanism in the presence of CaO nanoparticles has not yet been reported. However, one possible explanation for PLA/CaO showing a higher degradation rate than neat PLA is because there are absorbed hydroxyl groups on the surface of the nanoparticles, which are active in the breaking of chain reactions [109].

4. Conclusion

Poly(lactic acid) (PLA)/CaO nanocomposites were produced by the melting process. CaO nanoparticles were successfully synthesized with a diameter of 26.14 ± 3.31 nm, and then the surface was modified with oleic acid (Ol-CaO). The incorporation of Ol-CaO into the PLA improves the dispersion of the nanoparticles within the matrix polymer. The glass temperature (T_g) decreased ca. 13% for PLA/Ol-CaO compared to the neat PLA. The degree of crystallinity (X_c) for both PLA and nanocomposites remained almost constant, highlighting the amorphous structure of this material. However, the thermal stability for PLA/CaO and PLA/Ol-CaO nanocomposites decreased compared to the neat PLA (T_{max} ca. 23%) due to the catalytic activity of these nanoparticles. Even so, the values are still suitable for the applicability of these materials. Microhardness increased ca. 9% for PLA/Ol-CaO compared to the neat PLA due to the good dispersion of modified-surface Ol-CaO nanoparticles.

The antimicrobial activity of nanocomposites against *E. coli* bacteria reached 99.9% in PLA/Ol-CaO (8 wt.%). This behavior was attributed to the good distribution of modified nanoparticles within the PLA.

The influence of the incorporation of nanoparticles in the degradation of PLA was verified after five days of irradiation. After irradiation, the T_g of PLA and PLA/CaO nanocomposites decreased ca. 13% compared to neat PLA. The degree of crystallinity (X_c) increased, and this effect was higher for PLA/CaO (8 wt%) (ca. 7%), attributed to recrystallization of the polymer. The average molecular weight of viscous PLA decreased ca. 97% after the photodegradation test due to chain scissions and nanoparticles accelerated polymer degradation under irradiation, as observed by SEM.

The results found in this study demonstrate that these systems can be applied as functional, active, and degradable food packaging applications or medical devices.

Declaration of Competing Interest

The authors declare that they have no known competing financial interests or personal relationships that could have appeared to influence the work reported in this paper.

CRediT authorship contribution statement

Carlos Loyo: Conceptualization, Methodology. **Viviana Moreno-Serna:** Data curation, Writing – original draft. **Jairo Fuentes:** Methodology, Data curation, Investigation. **Nicolás Amigo:** Methodology, Data curation. **Francesca Antonella Sepúlveda:** Methodology, Validation, Data curation. **J. Andrés Ortiz:** Visualization, Investigation, Writing – review & editing. **Lina M. Rivas:** Methodology. **María Teresa Ulloa:** Validation, Data curation. **Rosario Benavente:** Data curation, Writing – review & editing. **Paula A. Zapata:** Supervision, Writing – review & editing, Investigation, Writing – original draft.

Acknowledgments

P.A. Zapata acknowledges the financial support under FONDECYT Regular Project 1170226. V. Moreno-Serna acknowledges the financial support of ANID FONDECYT Postdoctorado 3210077. J.A. Ortiz thanks the financial support of ANID FONDECYT Postdoctorado 3200296. P.A. Zapata and C. Loyo acknowledge the financial support of DICYT Proyecto 022141ZR_POSTDOC, USA2055, Vicerrectoría de Investigación, Desarrollo e Innovación, Universidad de Santiago de Chile.

Supplementary materials

Supplementary material associated with this article can be found, in the online version, at doi:10.1016/j.polymdegradstab.2022.109865.

References

[1] K.G. Harding, J.S. Dennis, H. von Blottnitz, S.T.L. Harrison, Environmental analysis of plastic production processes: comparing petroleum-based polypropylene and polyethylene with biologically-based poly-β-hydroxybutyric acid us-

ing life cycle analysis, J. Biotechnol. 130 (2007) 57–66, doi:10.1016/j.jbiotec.2007.02.012.
[2] D. Xanthos, T.R. Walker, International policies to reduce plastic marine pollution from single-use plastics (plastic bags and microbeads): a review, Mar. Pollut. Bull. 118 (2017) 17–26, doi:10.1016/j.marpolbul.2017.02.048.
[3] R.E.J. Schnurr, V. Alboiu, M. Chaudhary, R.A. Corbett, M.E. Quanz, K. Sankar, H.S. Srain, V. Thavarajah, D. Xanthos, T.R. Walker, Reducing marine pollution from single-use plastics (SUPs): a review, Mar. Pollut. Bull. 137 (2018) 157–171, doi:10.1016/j.marpolbul.2018.10.001.
[4] C. Fonseca, A. Ochoa, M.T. Ulloa, E. Alvarez, D. Canales, P.A. Zapata, Poly(lactic acid)/TiO2 nanocomposites as alternative biocidal and antifungal materials, Mater. Sci. Eng. C. 57 (2015) 314–320, doi:10.1016/j.msec.2015.07.069.
[5] I. Widiastuti, Polylactide nanocomposites for packaging materials: a review, in: AIP Conf. Proc, American Institute of Physics Inc., 2016, doi:10.1063/1.4941486.
[6] M.P. Arrieta, M.D. Samper, M. Aldas, J. López, On the use of PLA-PHB blends for sustainable food packaging applications, Materials (Basel) 10 (2017) 1–26, doi:10.3390/ma10091008.
[7] C. Fan, R. Cui, W. Lu, H. Chen, M. Yuan, Y. Qin, Effect of high pressure treatment on properties and nano–Ag migration of PLA-based food packaging film, Polym. Test. 76 (2019) 73–81, doi:10.1016/j.polymertesting.2019.03.005.
[8] L.K. Kian, N. Saba, M. Jawaid, M.T.H. Sultan, A review on processing techniques of bast fibers nanocellulose and its polylactic acid (PLA) nanocomposites, Int. J. Biol. Macromol. 121 (2019) 1314–1328, doi:10.1016/j.ijbiomac.2018.09.040.
[9] M. Ghozali, S. Fahmiati, E. Triwulandari, W.K. Restu, D. Farhan, M. Wulansari, W. Fatriasari, PLA/metal oxide biocomposites for antimicrobial packaging application, Polym. Technol. Mater. 59 (2020) 1332–1342, doi:10.1080/25740881.2020.1738475.
[10] C. Villegas, M.P. Arrieta, A. Rojas, A. Torres, S. Faba, M.J. Toledo, M.A. Gutierrez, E. Zavalla, J. Romero, M.J. Galotto, X. Valenzuela, PLA/organoclay bionanocomposites impregnated with thymol and cinnamaldehyde by supercritical impregnation for active and sustainable food packaging, Compos. Part B Eng. 176 (2019) 107336, doi:10.1016/j.compositesb.2019.107336.
[11] C. Silvestre, D. Duraccio, S. Cimmino, Food packaging based on polymer nanomaterials, Prog. Polym. Sci. 36 (2011) 1766–1782, doi:10.1016/j.progpolymsci.2011.02.003.
[12] C. Vasile, M. Rapa, M. Stefan, M. Stan, S. Macavei, R.N. Darie-Nita, L. Barbu-Tudoran, D.C. Vodnar, E.E. Popa, R. Stefan, G. Borodi, M. Brebu, New PLA/ZnO:cu/Ag bionanocomposites for food packaging, Express Polym. Lett. 11 (2017) 531–544. https://doi.org/10.3144/expresspolymlett.2017.51.
[13] Z. Kovačević, S. Bischof, E. Vujasinović, M. Fan, The potential of nanoclay modified Spartium junceum L. Fibres used as reinforcement in PLA matrix composites for automotive applications, Int. J. Nanotechnol. 15 (2018) 695–700, doi:10.1504/IJNT.2018.098436.
[14] Y.A. Arfat, J. Ahmed, A. Al Hazza, H. Jacob, A. Joseph, Comparative effects of untreated and 3-methacryloxypropyltrimethoxysilane treated ZnO nanoparticle reinforcement on properties of polylactide-based nanocomposite films, Int. J. Biol. Macromol. 101 (2017) 1041–1050, doi:10.1016/j.ijbiomac.2017.03.176.
[15] S. Marconi, G. Alaimo, V. Mauri, M. Torre, F. Auricchio, Impact of graphene reinforcement on mechanical properties of PLA 3D printed materials, in: 2017 IEEE MTT-S Int. Microw. Work. Ser. Adv. Mater. Process. RF THz Appl. IMWS-AMP 2017. 2018-Janua, 2018, pp. 1–3, doi:10.1109/IMWS-AMP.2017.8247414.
[16] D. Enescu, M.A. Cerqueira, P. Fucinos, L.M. Pastrana, Recent advances and challenges on applications of nanotechnology in food packaging. A literature review, Food Chem. Toxicol. 134 (2019) 110814, doi:10.1016/j.fct.2019.110814.
[17] K. Shameli, Mansor Bin Ahmad, Majid Darroudi, Russly Abdul Rahman, Maryam Jokar, Wan Md, Zin Wan Yunis, Nor Azowa Ibrahim, Silver/poly (lactic acid) nanocomposites: preparation, characterization, and antibacterial activity, Int. J. Nanomedicine. 5 (2010) 573, doi:10.2147/IJN.S12007.
[18] A. Marra, C. Silvestre, D. Duraccio, S. Cimmino, Polylactic acid/zinc oxide biocomposite films for food packaging application, Int. J. Biol. Macromol. 88 (2016) 254–262, doi:10.1016/j.ijbiomac.2016.03.039.
[19] H. Rodríguez-Tobías, G. Morales, D. Grande, Improvement of mechanical properties and antibacterial activity of electrospun poly(D,L-lactide)-based mats by incorporation of ZnO-graft-poly(D,L-lactide) nanoparticles, Mater. Chem. Phys. 182 (2016) 324–331, doi:10.1016/j.matchemphys.2016.07.039.
[20] E. Lizundia, M.C. Penayo, A. Guinault, J.L. Vilas, S. Domenek, Impact of ZnO nanoparticle morphology on relaxation and transport properties of PLA nanocomposites, Polym. Test. 75 (2019) 175–184, doi:10.1016/j.polymertesting.2019.02.009.
[21] E.A.S. González, D. Olmos, M.Á. Lorente, I. Vélaz, J. González-Benito, Preparation and Characterization of Polymer Composite Materials Based on PLA/TiO2 for Antibacterial Packaging, Polymers (Basel) 10 (2018) 1365, doi:10.3390/polym10121365.
[22] Z. Mirghiasi, F. Bakhtiari, E. Darezereshki, E. Esmaeilzadeh, Preparation and characterization of CaO nanoparticles from Ca(OH)2 by direct thermal decomposition method, J. Ind. Eng. Chem. 20 (2014) 113–117, doi:10.1016/j.jiec.2013.04.018.
[23] Y. Cao, J. Li, F. Liu, X. Li, Q. Jiang, S. Cheng, Y. Gu, Review or mini-review Consideration of interaction between nanoparticles and food components for the safety assessment of nanoparticles following oral exposure: a review, Environ. Toxicol. Pharmacol. 46 (2016) 206–210, doi:10.1016/j.etap.2016.07.023.
[24] P.K. Stoimenov, R.L. Klinger, G.L. Marchin, K.J. Klabunde, Metal oxide nanoparticles as bactericidal agents, Langmuir. 18 (2002) 6679–6686. https://doi.org/10.1021/la0202374.
[25] S.M. Dizaj, F. Lotfipour, M. Barzegar-Jalali, M.H. Zarrintan, K. Adibkia, Antimicrobial activity of the metals and metal oxide nanoparticles, Mater. Sci. Eng. C. 44 (2014) 278–284, doi:10.1016/j.msec.2014.08.031.
[26] J.F. Pereira, D.P. Ferreira, E. Pinho, R. Fangueiro, Chemical and biological warfare protection and self-decontaminating flax fabrics based on CaO nanoparticles, Key Eng. Mater. (2019) 75–83 812 KEM, doi:10.4028/www.scientific.net/KEM.812.75.
[27] G. Marquis, B. Ramasamy, S. Banwarilal, A.P. Munusamy, Evaluation of antibacterial activity of plant mediated CaO nanoparticles using Cissus quadrangularis extract, (2015). https://doi.org/10.1016/j.jphotobiol.2015.12.013.
[28] A. Roy, S.S. Gauri, M. Bhattacharya, J. Bhattacharya, Antimicrobial activity of CaO nanoparticles, J. Biomed. Nanotechnol. 9 (2013) 1570–1578, doi:10.1166/jbn.2013.1681.
[29] W.S. Mohamed, H.E. Nasr, R. Gutmann, R.A. Sobh, Effect of CaO Nanoparticles on the Properties of Polyamide 6, Egypt. J. Chem. 58 (2015) 365–375, doi:10.21608/ejchem.2015.1029.
[30] F. Bobillier, D. Canales, F. Antonella, A. Cament, L.M. Rivas, T. Ulloa, P. Reyes, J.A. Ortiz, G. Tatiana, C. Loyo, P.A. Zapata, Mechanical and Antimicrobial Polyethylene Composites with CaO Nanoparticles, Polymers (Basel) 12 (2020) 2132, doi:10.3390/polym12092132.
[31] Z. Liu, Y. Weng, Z. Huang, Y. Jin, J. Hu, D. Chou, S. Shao, Manufacture of a hydrophobic CaO/polylactic acid composite, Mater. Manuf. Process. 34 (2019) 303–311, doi:10.1080/10426914.2018.1512113.
[32] Z.X. Tang, Z. Yu, Z.L. Zhang, X.Y. Zhang, Q.Q. Pan, L.E. Shi, Sonication-assisted preparation of CaO nanoparticles for antibacterial agents, Quim. Nova. 36 (2013) 933–936, doi:10.1590/S0100-40422013000700002.
[33] Z. Li, Y. Zhu, Surface-modification of SiO 2 nanoparticles with oleic acid, Appl. Surf. Sci. 211 (2003) 315–320, doi:10.1016/S0169-4332(03)00259-9.
[34] D. Yañez, S. Guerrero, I. Lieberwirth, M.T. Ulloa, T. Gomez, F.M. Rabagliati, P.A. Zapata, Photocatalytic inhibition of bacteria by TiO2nanotubes-doped polyethylene composites, Appl. Catal. A Gen. 489 (2015) 255–261, doi:10.1016/j.apcata.2014.10.051.
[35] P.A. Amigo, N. Palza, H. Canales, D. Sepúlveda, F. Vasco, D.A. Sepúlveda, F. Zapata, Effect of starch nanoparticles on the crystallization kinetics and photodegradation of high density polyethylene, Compos. Part B Eng. 174 (2019) 106979, doi:10.1016/j.compositesb.2019.106979.
[36] B. Brüster, Y.O. Adjoua, R. Dieden, P. Grysan, C.E. Federico, V. Berthé, F. Addiego, Plasticization of polylactide with myrcene and limonene as bio-based plasticizers: conventional vs. reactive extrusion, Polymers (Basel) 11 (2019) 1363, doi:10.3390/polym11081363.
[37] D. Canales, M. Saavedra, M.T. Flores, J. Bejarano, J.A. Ortiz, P. Orihuela, A. Alfaro, E. Pabón, H. Palza, P.A. Zapata, Effect of bioglass nanoparticles on the properties and bioactivity of poly(lactic acid) films, J. Biomed. Mater. Res. - Part A. (2020) 2032–2043, doi:10.1002/jbm.a.36963.
[38] S. Therias, J.F. Larché, P.O. Bussière, J.L. Gardette, M. Murariu, P. Dubois, Photochemical Behavior of Polylactide/ZnO Nanocomposite Films, Biomacromolecules 13 (2012) 3283–3291, doi:10.1021/BM301071W.
[39] M. Gardette, S. Thérias, J.L. Gardette, M. Murariu, P. Dubois, Photooxidation of polylactide/calcium sulphate composites, Polym. Degrad. Stab. 96 (2011) 616–623, doi:10.1016/J.POLYMDEGRADSTAB.2010.12.023.
[40] E.T. Santos, C. Alfonsín, A.J.S. Chambel, A. Fernandes, A.P. Soares Dias, C.I.C. Pinheiro, M.F. Ribeiro, Investigation of a stable synthetic sol–gel CaO sorbent for CO_2 capture, Fuel 94 (2012) 624–628, doi:10.1016/j.fuel.2011.10.011.
[41] N. Asikin-Mijan, Y.H. Taufiq-Yap, H.V. Lee, Synthesis of clamshell derived Ca(OH)2 nano-particles via simple surfactant-hydration treatment, Chem. Eng. J. 262 (2015) 1043–1051, doi:10.1016/j.cej.2014.10.069.
[42] L. Habte, N. Shiferaw, D. Mulatu, T. Thenepalli, R. Chilakala, J.W. Ahn, Synthesis of nano-calcium oxide fromwaste eggshell by sol-gel method, Sustain 11 (2019) 3196, doi:10.3390/su11113196.
[43] P. Velusamy, S. Chia-Hung, A. Shritama, G.V. Kumar, V. Jeyanthi, K. Pandian, Synthesis of oleic acid coated iron oxide nanoparticles and its role in antibiofilm activity against clinical isolates of bacterial pathogens, J. Taiwan Inst. Chem. Eng. 59 (2016) 450–456, doi:10.1016/j.jtice.2015.07.018.
[44] F.A. Sepúlveda, F. Rivera, D. Canales, V. Moreno-Serna, R. Benavente, C. Loyo, L.M. Rivas, M.T. Ulloa, Ó. Gil-Castell, A. Ribes-Greus, J.A. Ortiz, P.A. Zapata, Poly(lactic acid)/D-limonene/ZnO bio-nanocomposites with antimicrobial properties, J. Appl. Polym. Sci. 139 (2022) e51542, doi:10.1002/app.51542.
[45] A. ROY, J. BHATTACHARYA, MICROWAVE-ASSISTED SYNTHESIS AND CHARACTERIZATION OF CaO NANOPARTICLES, Int. J. Nanosci. 10 (2011) 413–418, doi:10.1142/S0219581x11008150.
[46] T. Liu, Y. Zhu, X. Zhang, T. Zhang, T. Zhang, X. Li, Synthesis and characterization of calcium hydroxide nanoparticles by hydrogen plasma-metal reaction method, Mater. Lett. 64 (2010) 2575–2577, doi:10.1016/j.matlet.2010.08.050.
[47] K. Rojas, D. Canales, N. Amigo, L. Montoille, A. Cament, L.M. Rivas, O. Gil-Castell, P. Reyes, M.T. Ulloa, A. Ribes-Greus, P.A. Zapata, Effective antimicrobial materials based on low-density polyethylene (LDPE) with zinc oxide (ZnO) nanoparticles, Compos. Part B Eng. 172 (2019) 173–178, doi:10.1016/j.compositesb.2019.05.054.
[48] B. Smith, Infrared Spectral Interpretation: A Systematic Approach, CRC Press, 1998 First edit.
[49] L. Robinet, M.C. Corbeil, The characterization of metal soaps, Stud. Conserv. 48 (2003) 23–40, doi:10.1179/sic.2003.48.1.23.
[50] Y. Wang, W. Eli, Y. Liu, L. Long, Synthesis of Environmentally Friendly Calcium Oleate Detergent, Ind. Eng. Chem. Res. 47 (2008) 8561–8565, doi:10.1021/ie800679a.

[51] C.Y. Wang, J.M. Hong, G. Chen, Y. Zhang, N. Gu, Facile method to synthesize oleic acid-capped magnetite nanoparticles, Chinese Chem. Lett. 21 (2010) 179–182, doi:10.1016/j.cclet.2009.10.024.
[52] R.M. Patil, P.B. Shete, N.D. Thorat, S.V. Otari, K.C. Barick, A. Prasad, R.S. Ningthoujam, B.M. Tiwale, S.H. Pawar, Non-aqueous to aqueous phase transfer of oleic acid coated iron oxide nanoparticles for hyperthermia application, RSC Adv 4 (2014) 4515–4522, doi:10.1039/C3RA44644A.
[53] Z. Li, Y. Zhu, Surface-modification of SiO2 nanoparticles with oleic acid, Appl. Surf. Sci. 211 (2003) 315–320, doi:10.1016/S0169-4332(03)00259-9.
[54] Y. Gao, G. Chen, Y. Oli, Z. Zhang, Q. Xue, Study on tribological properties of oleic acid-modified TiO2 nanoparticle in water, Wear 252 (2002) 454–458, doi:10.1016/S0043-1648(01)00891-2.
[55] A.A. Baharuddin, B.C. Ang, N.A. Abu Hussein, A. Andriyana, Y.H. Wong, Mechanisms of highly stabilized ex-situ oleic acid-modified iron oxide nanoparticles functionalized with 4-pentynoic acid, Mater. Chem. Phys. 203 (2018) 212–222, doi:10.1016/j.matchemphys.2017.09.051.
[56] A. Buzarovska, S. Dinescu, L. Chitoiu, M. Costache, Porous poly(l-lactic acid) nanocomposite scaffolds with functionalized TiO2 nanoparticles: properties, cytocompatibility and drug release capability, J. Mater. Sci. 53 (2018) 11151–11166, doi:10.1007/s10853-018-2415-0.
[57] B. Shentu, J. LI, Z. Weng, Effect of Oleic Acid-modified Nano-CaCO3 on the Crystallization Behavior and Mechanical Properties of Polypropylene, Chinese J. Chem. Eng. 14 (2006) 814–818, doi:10.1016/s1004-9541(07)60018-4.
[58] S.C. Cifuentes, E. Frutos, J.L. González-Carrasco, M. Muñoz, M. Multigner, J. Chao, R. Benavente, M. Lieblich, Novel PLLA/magnesium composite for orthopedic applications: a proof of concept, Mater. Lett. 74 (2012) 239–242, doi:10.1016/j.matlet.2012.01.134.
[59] A. Zhu, H. Diao, Q. Rong, A. Cai, Preparation and properties of polylactide–silica nanocomposites, J. Appl. Polym. Sci. 116 (2010) 2866–2873, doi:10.1002/app.31786.
[60] M. Nofar, Effects of nano-/micro-sized additives and the corresponding induced crystallinity on the extrusion foaming behavior of PLA using supercritical CO_2, Mater. Des. 101 (2016) 24–34, doi:10.1016/j.matdes.2016.03.147.
[61] P.O. Bussiere, S. Therias, J.-.L. Gardette, M. Murariu, P. Dubois, M. Baba, Effect of ZnO nanofillers treated with triethoxy caprylylsilane on the isothermal and non-isothermal crystallization of poly(lactic acid), Phys. Chem. Chem. Phys. 14 (2012) 12301, doi:10.1039/c2cp41574g.
[62] H. Zhang, J. Huang, L. Yang, R. Chen, W. Zou, X. Lin, J. Qu, Preparation, characterization and properties of PLA/TiO2 nanocomposites based on a novel vane extruder, RSC Adv 5 (2014) 4639–4647, doi:10.1039/C4RA14538K.
[63] K. Fukushima, C. Abbate, D. Tabuani, M. Gennari, G. Camino, Biodegradation of poly(lactic acid) and its nanocomposites, Polym. Degrad. Stab. 94 (2009) 1646–1655, doi:10.1016/j.polymdegradstab.2009.07.001.
[64] S.C. Cifuentes, E. Frutos, R. Benavente, V. Lorenzo, J.L. González-Carrasco, Assessment of mechanical behavior of PLA composites reinforced with Mg micro-particles through depth-sensing indentations analysis, J. Mech. Behav. Biomed. Mater. 65 (2017) 781–790, doi:10.1016/j.jmbbm.2016.09.013.
[65] P.J. Jandas, S. Mohanty, S.K. Nayak, Thermal properties and cold crystallization kinetics of surface-treated banana fiber (BF)-reinforced poly(lactic acid) (PLA) nanocomposites, J. Therm. Anal. Calorim. 114 (2013) 1265–1278, doi:10.1007/s10973-013-3102-7.
[66] L.B. Ding, J. Rui, J.T. Li, The Effect of Nanoparticles Modification on PLA/Nano-ZnO Composite, Appl. Mech. Mater. 420 (2013) 230–233, doi:10.4028/www.scientific.net/AMM.420.230.
[67] E. Perez, J.M. Perefia, R. Benavente, A. Bello, V. Lorenzo, Microhardness and DSC measurements on liquid crystalline poly(diethylene glycol p, p'-bibenzoate) as a function of the ageing time, Polym. Bull. 29 (1992) 233–237, doi:10.1007/bf00558062.
[68] Y.C. Zhang, J.F. Xie, H.Y. Wu, Y.P. Qiu, Crystallization and Mechanical Properties of Nano ZnO/PP/PLA Composite Filaments, Mater. Sci. Forum. 620–622 (2009) 485–488, doi:10.4028/www.scientific.net/MSF.620-622.485.
[69] A.M. Harris, E.C. Lee, Improving mechanical performance of injection molded PLA by controlling crystallinity, J. Appl. Polym. Sci. 107 (2008) 2246–2255, doi:10.1002/app.27261.
[70] M.A. Ortenzi, L. Basilissi, H. Farina, G. Di Silvestro, L. Piergiovanni, E. Mascheroni, Evaluation of crystallinity and gas barrier properties of films obtained from PLA nanocomposites synthesized via "in situ" polymerization of L-lactide with silane-modified nanosilica and montmorillonite, Eur. Polym. J. 66 (2015) 478–491, doi:10.1016/j.eurpolymj.2015.03.006.
[71] D.S. Chaudhary, R. Prasad, R.K. Gupta, S.N. Bhattacharya, Clay intercalation and influence on crystallinity of EVA-based clay nanocomposites, Thermochim. Acta. 433 (2005) 187–195, doi:10.1016/j.tca.2005.02.031.
[72] M. Ramos, E. Fortunati, M. Peltzer, F. Dominici, A. Jiménez, M. del C. Garrigós, J.M. Kenny, Influence of thymol and silver nanoparticles on the degradation of poly(lactic acid) based nanocomposites: thermal and morphological properties, Polym. Degrad. Stab. 108 (2014) 158–165, doi:10.1016/j.polymdegradstab.2014.02.011.
[73] Y. Fan, H. Nishida, S. Hoshihara, Y. Shirai, Y. Tokiwa, T. Endo, Pyrolysis kinetics of poly(L-lactide) with carboxyl and calcium salt end structures, Polym. Degrad. Stab. 79 (2003) 547–562, doi:10.1016/S0141-3910(02)00374-9.
[74] Y. Fan, H. Nishida, T. Mori, Y. Shirai, T. Endo, Thermal degradation of poly(L-lactide): effect of alkali earth metal oxides for selective L,L-lactide formation, Polymer (Guildf) 45 (2004) 1197–1205, doi:10.1016/j.polymer.2003.12.058.
[75] Y. Fan, H. Nishida, Y. Shirai, T. Endo, Racemization on thermal degradation of poly(L-lactide) with calcium salt end structure, Polym. Degrad. Stab. 80 (2003) 503–511, doi:10.1016/S0141-3910(03)00033-8.
[76] C. Wang, Y. Liu, H. Bala, Y. Pan, J. Zhao, X. Zhao, Z. Wang, Facile preparation of CaCO3 nanoparticles with self-dispersing properties in the presence of dodecyl dimethyl betaine, Colloids Surfaces A Physicochem. Eng. Asp. 297 (2007) 179–182, doi:10.1016/j.colsurfa.2006.10.045.
[77] J. Yu, J. Yu, Z. Guo, Y. Gao, Preparation of CaCO3/Polystyrene Inorganic/Organic Composite Nanoparticles, Macromol. Rapid Commun. 22 (2001) 1261–1264, doi:10.1002/1521-3927(20011001)22:15⟨1261::AID-MARC1261⟩3.0.CO;2-7.
[78] L. Feng, S. Feng, X. Bian, G. Li, X. Chen, Pyrolysis mechanism of Poly(lactic acid) for giving lactide under the catalysis of tin, Polym. Degrad. Stab. 157 (2018) 212–223, doi:10.1016/j.polymdegradstab.2018.10.008.
[79] X. jie Wang, Z. Huang, M. yu Wei, T. Lu, D. dan Nong, J. xu Zhao, X. yang Gao, L. jun Teng, Catalytic effect of nanosized ZnO and TiO2 on thermal degradation of poly(lactic acid) and isoconversional kinetic analysis, Thermochim. Acta. 672 (2019) 14–24, doi:10.1016/j.tca.2018.12.008.
[80] M. Garg, S.R. White, N.R. Sottos, Rapid Degradation of Poly(lactic acid) with Organometallic Catalysts, ACS Appl. Mater. Interfaces. 11 (2019) 46226–46232, doi:10.1021/acsami.9b17599.
[81] F.A. Sepúlveda, F. Rivera, C. Loyo, D. Canales, V. Moreno-Serna, R. Benavente, L.M. Rivas, M.T. Ulloa, O. Gil-Castell, A. Ribes-Greus, J.A. Ortiz, P.A. Zapata, Poly (lactic acid)/D-limonene/ZnO bio-nanocomposites with antimicrobial properties, J. Appl. Polym. Sci. (2021) 51542, doi:10.1002/APP.51542.
[82] M. Murariu, A. Doumbia, L. Bonnaud, A.L. Dechief, Y. Paint, M. Ferreira, C. Campagne, E. Devaux, P. Dubois, High-performance polylactide/ZnO nanocomposites designed for films and fibers with special end-use properties, Biomacromolecules 12 (2011) 1762–1771, doi:10.1021/bm2001445.
[83] C. Chen, R.S. Justice, D.W. Schaefer, J.W. Baur, Highly dispersed nanosilica-epoxy resins with enhanced mechanical properties, Polymer (Guildf). 49 (2008) 3805–3815. https://doi.org/10.1016/j.polymer.2008.06.023.
[84] H. Liu, T.J. Webster, Mechanical properties of dispersed ceramic nanoparticles in polymer composites for orthopedic applications, Int. J. Nanomedicine. 5 (2010) 299–313, doi:10.2147/ijn.s9882.
[85] L.D. Aguilera-Camacho, C. Hernández-Navarro, K.J. Moreno, J.S. García-Miranda, A. Arizmendi-Morquecho, Improvement effects of CaO nanoparticles on tribological and microhardness properties of PMMA coating, J. Coatings Technol. Res. 12 (2015) 347–355, doi:10.1007/s11998-014-9639-y.
[86] E.A. Münchow, D. Pankajakshan, M.T.P. Albuquerque, K. Kamocki, E. Piva, R.L. Gregory, M.C. Bottino, Synthesis and characterization of CaO-loaded electrospun matrices for bone tissue engineering, Clin. Oral Investig. 20 (2016) 1921–1933, doi:10.1007/s00784-015-1671-5.
[87] C.E. Tanase, I. Spiridon, PLA/chitosan/keratin composites for biomedical applications, Mater. Sci. Eng. C. 40 (2014) 242–247, doi:10.1016/j.msec.2014.03.054.
[88] A. Ostafinska, I. Fortelný, J. Hodan, S. Krejčíková, M. Nevoralová, J. Kredatusová, Z. Kruliš, J. Kotek, M. Šlouf, Strong synergistic effects in PLA/PCL blends: impact of PLA matrix viscosity, J. Mech. Behav. Biomed. Mater. 69 (2017) 229–241, doi:10.1016/j.jmbbm.2017.01.015.
[89] H.A. Sallal, A.A. Abdul-Hamead, F.M. Othman, Effect of nano powder (Al2O3-CaO) addition on the mechanical properties of the polymer blend matrix composite, Def. Technol. 16 (2020) 425–431, doi:10.1016/j.dt.2019.07.013.
[90] J. Sawai, T. Yoshikawa, Quantitative evaluation of antifungal activity of metallic oxide powders (MgO, CaO and ZnO) by an indirect conductimetric assay, J. Appl. Microbiol. 96 (2004) 803–809, doi:10.1111/j.1365-2672.2004.02234.x.
[91] C.J. Hewitt, S.R. Bellara, A. Andreani, G. Nebe-von-Caron, C.M. McFarlane, An evaluation of the anti-bacterial action of ceramic powder slurries using multi-parameter flow cytometry, Biotechnol. Lett. 23 (2001) 667–675, doi:10.1023/A:1010379714673.
[92] A. Khezerlou, M. Alizadeh-Sani, M. Azizi-Lalabadi, A. Ehsani, Nanoparticles and their antimicrobial properties against pathogens including bacteria, fungi, parasites and viruses, Microb. Pathog. 123 (2018) 505–526, doi:10.1016/j.micpath.2018.08.008.
[93] G. Gedda, S. Pandey, Y.-.C. Lin, H.-.F. Wu, Antibacterial effect of calcium oxide nano-plates fabricated from shrimp shells, Green Chem 17 (2015) 3276–3280, doi:10.1039/C5GC00615E.
[94] B. Gharpure, Saee, Aman Akash, Ankamwar, A Review on Antimicrobial Properties of Metal Nanoparticles, J. Nanosci. Nanotechnol. 20 (2020) 3303–3339, doi:10.1166/jnn.2020.17677.
[95] S.M. Dizaj, F. Lotfipour, M. Barzegar-Jalali, M.H. Zarrintan, K. Adibkia, Antimicrobial activity of the metals and metal oxide nanoparticles, Mater. Sci. Eng. C. 44 (2014) 278–284, doi:10.1016/J.MSEC.2014.08.031.
[96] H. Tsuji, Y. Echizen, Y. Nishimura, Photodegradation of biodegradable polyesters: a comprehensive study on poly(l-lactide) and poly(ε-caprolactone), Polym. Degrad. Stab. 91 (2006) 1128–1137, doi:10.1016/J.POLYMDEGRADSTAB.2005.07.007.
[97] P. Mróz, S. Białas, M. Mucha, H. Kaczmarek, Thermogravimetric and DSC testing of poly(lactic acid) nanocomposites, Thermochim. Acta. 573 (2013) 186–192, doi:10.1016/j.tca.2013.09.012.
[98] Y. Luo, Y. Cao, G. Guo, Effects of TiO2 nanoparticles on the photodegradation of poly(lactic acid), J. Appl. Polym. Sci. 135 (2018) 1–8, doi:10.1002/app.46509.
[99] I.Y. Denisyuk, S.A. Pozdnyakova, I.G. Koryakina, M.V. Uspenskaya, K.V. Volkova, Polymer photodegradation initiated by ZnO nanoparticles, Opt. Spectrosc. (English Transl. Opt. i Spektrosk. 121 (2016) 778–781, doi:10.1134/S0030400x16110096.
[100] G. Gorrasi, A. Sorrentino, Photo-oxidative stabilization of carbon nanotubes on polylactic acid, Polym. Degrad. Stab. 98 (2013) 963–971, doi:10.1016/J.POLYMDEGRADSTAB.2013.02.012.
[101] G. Gorrasi, C. Milone, E. Piperopoulos, M. Lanza, A. Sorrentino, Hybrid clay mineral-carbon nanotube-PLA nanocomposite films. Preparation and pho-

todegradation effect on their mechanical, thermal and electrical properties, Appl. Clay Sci. 71 (2013) 49–54, doi:10.1016/J.CLAY.2012.11.004.
[102] P. Pan, W. Kai, B. Zhu, T. Dong, Y. Inoue, Polymorphous Crystallization and Multiple Melting Behavior of Poly(l-lactide): Molecular Weight Dependence, Macromolecules 40 (2007) 6898–6905, doi:10.1021/ma071258d.
[103] S. Benali, S. Aouadi, A.-.L. Dechief, M. Murariu, P. Dubois, Key factors for tuning hydrolytic degradation of polylactide/zinc oxide nanocomposites, Nanocomposites 1 (2015) 51–61, doi:10.1179/2055033214Y.0000000007.
[104] M. Murariu, Y. Paint, O. Murariu, J.-.M. Raquez, L. Bonnaud, P. Dubois, Current progress in the production of PLA–ZnO nanocomposites: beneficial effects of chain extender addition on key properties, J. Appl. Polym. Sci. 132 (2015) 1–11, doi:10.1002/app.42889.
[105] Z. Liu, S. Chen, J. Zhang, Photodegradation of ethylene–octene copolymers with different octene contents, Polym. Degrad. Stab. 96 (2011) 1961–1972, doi:10.1016/J.POLYMDEGRADSTAB.2011.08.009.
[106] W. Chávez-Montes, G. González-Sánchez, E. López-Martínez, P. de Lira-Gómez, L. Ballinas-Casarrubias, S. Flores-Gallardo, Effect of Artificial Weathering on PLA/Nanocomposite Molecular Weight Distribution, Polymers (Basel) 7 (2015) 760–776, doi:10.3390/polym7040760.
[107] G. Lo Re, S. Benali, Y. Habibi, J.-.M. Raquez, P. Dubois, Stereocomplexed PLA nanocomposites: from in situ polymerization to materials properties, Eur. Polym. J. 54 (2014) 138–150, doi:10.1016/j.eurpolymj.2014.03.004.
[108] J. Salač, J. Šerá, M. Juřa, V. Verney, A.A. Marek, M. Koutný, Photodegradation and biodegradation of poly(lactic) acid containing orotic acid as a nucleation agent, Materials (Basel) 12 (2019), doi:10.3390/ma12030481.
[109] J. Li, R. Yang, J. Yu, Y. Liu, Natural photo-aging degradation of polypropylene nanocomposites, Polym. Degrad. Stab. 93 (2008) 84–89, doi:10.1016/j.polymdegradstab.2007.10.022.
[110] P.A. Zapata, H. Palza, B. Díaz, A. Armijo, F. Sepúlveda, J.A. Ortiz, M.P. Ramírez, C. Oyarzún, Effect of CaCO3 nanoparticles on the mechanical and photodegradation properties of LDPE, Molecules 24 (2019) 1–12, doi:10.3390/molecules24010126.
[111] X. Liu, S. Khor, E. Petinakis, L. Yu, G. Simon, K. Dean, S. Bateman, Effects of hydrophilic fillers on the thermal degradation of poly(lactic acid), Thermochim. Acta. 509 (2010) 147–151, doi:10.1016/j.tca.2010.06.015.
[112] S. Ubeda, M. Aznar, C. Nerín, Determination of volatile compounds and their sensory impact in a biopolymer based on polylactic acid (PLA) and polyester, Food Chem 294 (2019) 171–178, doi:10.1016/j.foodchem.2019.05.069.
[113] M. de L. Ruiz Peralta, M. Sánchez-Cantú, E. Puente-López, E. Rubio-Rosas, F. Tzompantzi, Evaluation of calcium oxide in Rhodamine 6 G photodegradation, Catal. Today. 305 (2018) 75–81, doi:10.1016/j.cattod.2017.09.057.
[114] T. Kornprobst, J. Plank, Photodegradation of rhodamine B in presence of CaO and NiO-CaO catalysts, Int. J. Photoenergy. (2012) 1–7 2012, doi:10.1155/2012/398230.
[115] P.-.O. Bussière, J. Peyroux, G. Chadeyron, S. Therias, Influence of functional nanoparticles on the photostability of polymer materials: recent progress and further applications, Polym. Degrad. Stab. 98 (2013) 2411–2418, doi:10.1016/j.polymdegradstab.2013.06.009.
[116] A. Marra, G. Rollo, S. Cimmino, C. Silvestre, Assessment on the Effects of ZnO and Coated ZnO Particles on iPP and PLA Properties for Application in Food Packaging, Coatings 7 (2017) 29, doi:10.3390/coatings7020029.
[117] M. Gardette, S. Thérias, J.-.L. Gardette, M. Murariu, P. Dubois, Photooxidation of polylactide/calcium sulphate composites, Polym. Degrad. Stab. 96 (2011) 616–623, doi:10.1016/j.polymdegradstab.2010.12.023.
[118] S. Therias, J.-.F. Larché, P.-.O. Bussière, J.-.L. Gardette, M. Murariu, P. Dubois, Photochemical Behavior of Polylactide/ZnO Nanocomposite Films, Biomacromolecules 13 (2012) 3283–3291, doi:10.1021/bm301071w.